

Feasibility of a radiation-cooled scraper for the PXIE MEBT

C. Baffes¹, A. Denisov², A. Shemyakin^{1}*

¹ Fermilab[#], Batavia, IL 60510 USA

² Novosibirsk State University, 2 Pirogova Str., Novosibirsk, 630090 Russia. Summer student of Fermilab's PARTI program

September 11, 2013

Abstract

The PXIE MEBT will have a system of 16 scrapers for protection and collimation with a desired power rating of ~100W per jaw. This paper suggests an option of a radiation-cooled scraper and analyzes as a possible prototype an electrically isolated, Molybdenum alloy TZM plate. Such a plate was successfully tested at an electron beam test stand with scraping up to 100W from a high-power-density electron beam. The surface temperature of the plate was analyzed from the thermal radiation using a narrow-band red filter and a camera and was found in good agreement with ANSYS simulations. Results of preliminary measurements with a larger-size electron beam are in agreement with TZM emissivity of 0.13.

The preliminary conclusion from these tests and simulations for the PXIE is that the tested design can be used at an operation power rating of ~50W.

[#] Fermilab is operated by Fermi Research Alliance, LLC, under Contract DE-AC02-07CH11359 with the U.S. DOE

* shemyakin@fnal.gov

1 Table of Contents

2	Introduction	3
3	Radiation-cooled scraper	4
3.1	Preliminary estimations.....	5
3.1.1	Steady state temperature	5
3.1.2	Thermal expansion.....	5
3.1.3	Heat flow through the holder	5
4	ANSYS simulation for the PXIE case	6
4.1	Simulation parameters.....	6
4.1.1	Mesh.....	6
4.1.2	Beam Modeling.....	7
4.1.3	Thermal Parameters	8
4.2	Temperature distribution and mechanical stresses.....	9
4.2.1	Steady State Thermal Analysis	9
4.2.2	Structural Analysis.....	9
4.3	Conclusions from the ANSYS simulations.....	11
5	Testing of the scraper prototype with an electron beam.....	12
5.1	Test stand.....	12
5.2	OTR measurements	13
5.3	Thermal radiation measurements	14
5.4	Power reflection	14
5.5	Measurements with a large size beam.....	15
5.5.1	Steady state spatial distribution	17
5.5.2	Temporal temperature dependence	17
5.5.3	Results of measurements with the large beam.....	18
5.6	Scraping of a high-power-density beam.....	19
5.6.1	ANSYS simulation for the test stand case of high-power-density beam scraping .	19
5.6.2	Measurements of high-power-density beam scraping	20
6	Discussion.....	22
7	Summary.....	22
8	Acknowledgements	23
9	Bibliography	23

2 Introduction

A multi-MW proton facility, Project X, has been proposed and is currently under development at Fermilab [1]. The concept for the Project X front end will be tested by carrying out an R&D program known as the Project X Injector Experiment (PXIE) [2]. PXIE consists of an H- ion source (IS); a Low Energy Beam Transport (LEBT); a CW 2.1-MeV RFQ; a Medium Energy Beam Transport (MEBT); two SRF cryomodules operating at 2K - a Half Wave Resonator (HWR) and a Single Spoke Resonator (SSR1); a High Energy Beam Transport (HEBT); and a beam dump (Figure 1).

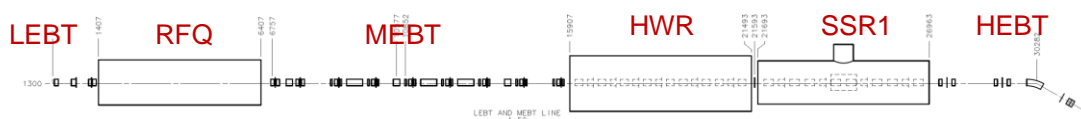


Figure 1: PXIE layout.

One of the research goals for the PXIE is to test the concept of protecting the SRF cavities from damage by the powerful, nearly CW beam. Part of the proposed protection system is 16 scrapers located in the MEFT (Fig.2).

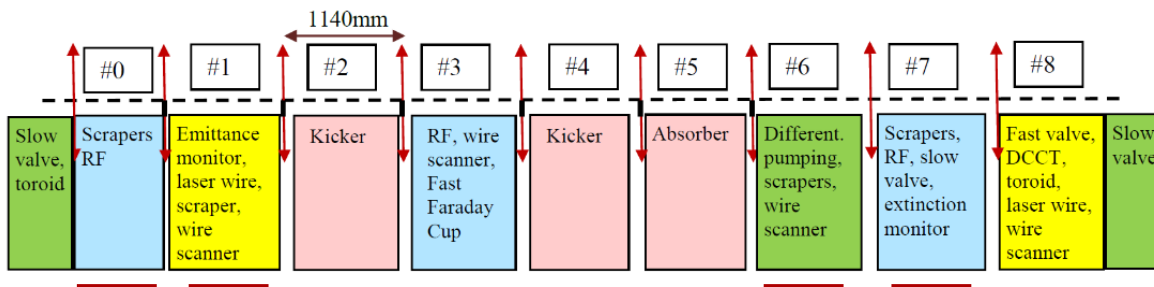


Figure 2: MEFT scheme. Arrows represent quadrupole doublets and triplets. Location of scrapers is underlined.

The scrapers are concentrated in two locations. Scrapers in the upstream location (sections #0 and #1 in Figure 2) provide initial scraping and protection of sensitive MEFT components (first of all, kickers), while in the downstream location, scraping is limited by requirements of high vacuum near SRF, and the main scraper function is protection. To ensure reliable removal of beam tails, each location contains two sets of scrapers (4 scrapers in each set) separated by $\sim 90^\circ$ of transverse phase advance. Each scraper is envisioned as an independently movable, electrically isolated plate with the surface facing the beam (“jaw”) being flat.

Preliminary estimations of beam tails show that scraping of $\sim 1\%$ of the beam, or $\sim 100\text{W}$ per scraper plate should satisfy the PXIE needs. An additional requirement is to avoid blistering that can result from irradiation by H- ions. Similarly to the MEFT absorber [3], this can be achieved by choosing the Molybdenum alloy TZM as the material of the scraper surface.

For an experimental facility such as the PXIE, where human and equipment errors will be part of the learning curve, it is important to have an error – tolerant design of scrapers, so that, for example, accidental missteering of the beam onto the scraper would not have dramatic consequences for the facility.

Finally, at that stage of the project it may be wise to sacrifice the scraper performance (i.e. power rating or position accuracy) to simplify the design and make it cheaper. This paper considers probably the simplest possible approach, where the scraper is an electrically isolated, rectangular TZM plate mounted on a linear drive, and power intercepted by the plate is removed by radiation. We present estimations and simulations of this case as well as results of testing the concept with an electron beam.

3 Radiation-cooled scraper

For estimations and simulations, we use parameters of a TZM plate that was used as a prototype in measurements with an electron beam (Figure 3). The plate dimensions and TZM properties are summarized in Table 1.

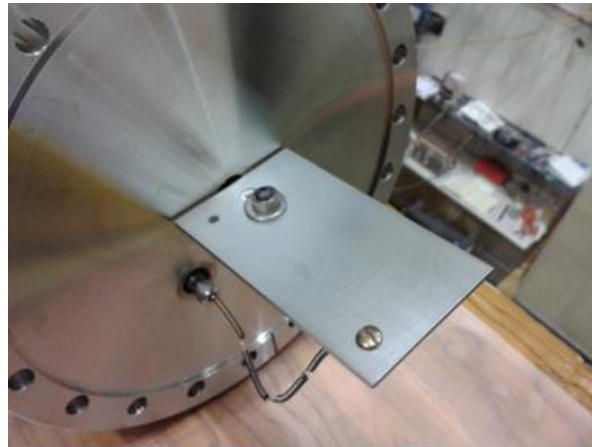


Figure 3: Photo of the TZM plate used as a prototype of a radiation-cooled scraper on the test stand. The plate current was measured through the wire seen at the lower part of the photo.

Table 1 Main properties of the TZM scraper prototype.

Sizes:	50.6 mm × 88.9 mm × 2 mm
Material:	Molybdenum alloy – TZM
Density:	10.16 g/cm ³
Heat capacity:	255 $\frac{J}{K \cdot kg}$
Thermal diffusivity:	0.455 cm ² /s
Thermal expansion:	~5.5 · 10 ⁻⁶ K ⁻¹
Melting point	2620 °C

3.1 Preliminary estimations

3.1.1 Steady state temperature

A rough estimation of a steady state scraper temperature can be made assuming that the scraper is heated evenly. The radiated power can be calculated with the Stefan-Boltzmann law:

$$W_{absorbed} = \varepsilon \sigma T^4 \cdot 2S, \quad (1)$$

where ε is emissivity, $S = 45 \text{ cm}^2$ is the scraper side area, σ is the Stefan's constant, and the factor of 2 indicates that both scraper sides are emitting. At emissivity 0.1 and the absorbed power 100 W, Eq.(1) gives the steady state temperature $\sim 1200 \text{ K}$. This temperature is far from the melting point ($\sim 2600 \text{ }^\circ\text{C}$ for TZM), hence it might be feasible to use such scraper at PXIE.

For simulation of the scraper thermal regime, the biggest uncertainty is the value of the plate emissivity. Depending on surface preparation, emissivity can range from 0.05 to 0.2 [4]. For example, in estimation by Eq.(1) this uncertainty corresponds to the range of equilibrium temperatures from 1000 K to 1400 K. Attempt to estimate the emissivity of the existing plate with a better accuracy was one the main reasons for measurements described in Section 5.

The prototype plate was cut from a blank of TZM 364 formed by a powder metallurgy process. All cuts were made using a wire-EDM machine, which leaves a recast layer approximately $20 \mu\text{m}$ thick. TZM is a brittle material; as such its strength is influenced by the number and character of surface flaws. The EDM recast layer is flaw-rich; it is therefore desirable to remove it. For the prototype plate, this was done using Scotchbrite abrasive on all surfaces. The result was a visually diffuse surface, though as described in Section 5.2 quasi-specular reflections were observed in testing. It is estimated the surface roughness was $R_a \leq \sim 1 \mu\text{m}$.

3.1.2 Thermal expansion

Position of the scraping edge depends, in part, on thermal expansion of the scraper plate when it is being heated. For the parameters indicated in Table 1 and the temperature increase of 1000 K, the thermal expansion is $\sim 0.5 \text{ mm}$. Though this value is significantly lower than the rms beam radius expected at PXIE ($\sim 2 \text{ mm}$), this effect certainly should be taken into account (see Section 6).

3.1.3 Heat flow through the holder

At the test stand, the scraper position inside the vacuum chamber is adjusted by a linear drive. The scraper plate is attached to the stainless steel rod of the drive through a ceramic plate that provides an electrical isolation. The upper estimation for the heat loss through the holder can be made assuming that the temperature drops only across ceramics. At the temperature difference of $\sim 1000 \text{ K}$, the heat flow is $< 10 \text{ W}$. A corresponding correction for the steady state temperature in Eq.(1) is $\sim 30 \text{ K}$.

To simplify the simulations of the scraper thermal regime, this effect was considered negligible and was not taken into account. Note that while a real temperature distribution was likely affected near the holder, temperature in this region was already low to be detected in thermal radiation measurements.

4 ANSYS simulation for the PXIE case

4.1 Simulation parameters

Using the geometry of the prototype (Figure 3), a FEA model was constructed to represent the PXIE scenario. ANSYS workbench 14.0 [5] was used. Key simulation parameters are shown in Table 2.

Table 2. Parameters of ANSYS simulations of the radiation – cooled scraper for the PXIE case.

Scraper Properties	
Plate Size	88.9 X 50.6 X 2mm (prototype dimensions)
Material	Molybdenum TZM 363/364 Temperature-dependent properties per [6]
Emissivity	0.1 over all temperatures
H- Beam Properties (PXIE Beam)	
Beam current	10 mA
Beam energy	2.1 MeV
Total beam power	21 kW
σ_x, σ_y	2 mm
Beam/Scraper Interaction Parameters	
Beam incidence	Normal incidence beam strikes the middle of the 50.6mm edge
Distance between the beam center and scraper edge	$2.75\sigma = 5.5 \text{ mm}$
Power absorption	100% (i.e. no reflection)
Scraped power	63 W
Peak power density	18.4 W/mm^2
Ambient temperature for radiation exchange with environment	300°K

4.1.1 Mesh

A half-symmetric 3D model was built, with the beam incident at the plane of symmetry. Zero-displacement constraints were applied to the side of the scraper opposite the beam interaction region. These constraints were applied kinematically – they do not introduce stresses with thermal expansion of the scraper. Symmetry and displacement constraints are shown in Figure 4.

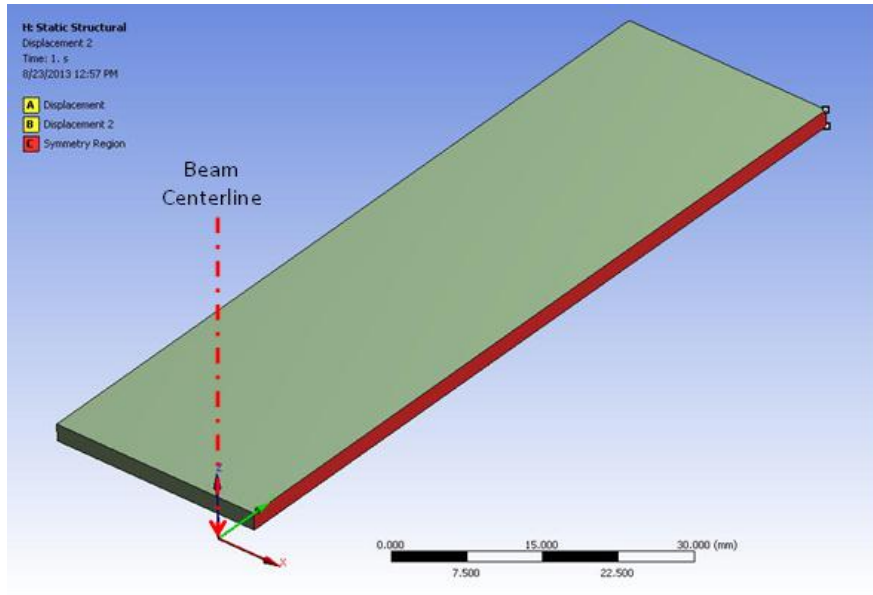


Figure 4: Underlying solid geometry of simulation, with symmetry plane (red) and displacement constraints (yellow).

The volume was meshed using 20-node quad elements, with 5 elements through the thickness of the scraper. In the beam interaction region, transverse element size is as small as $75\mu\text{m}$ to allow for smooth mapping of the beam heat load. The mesh used is shown in Figure 5.

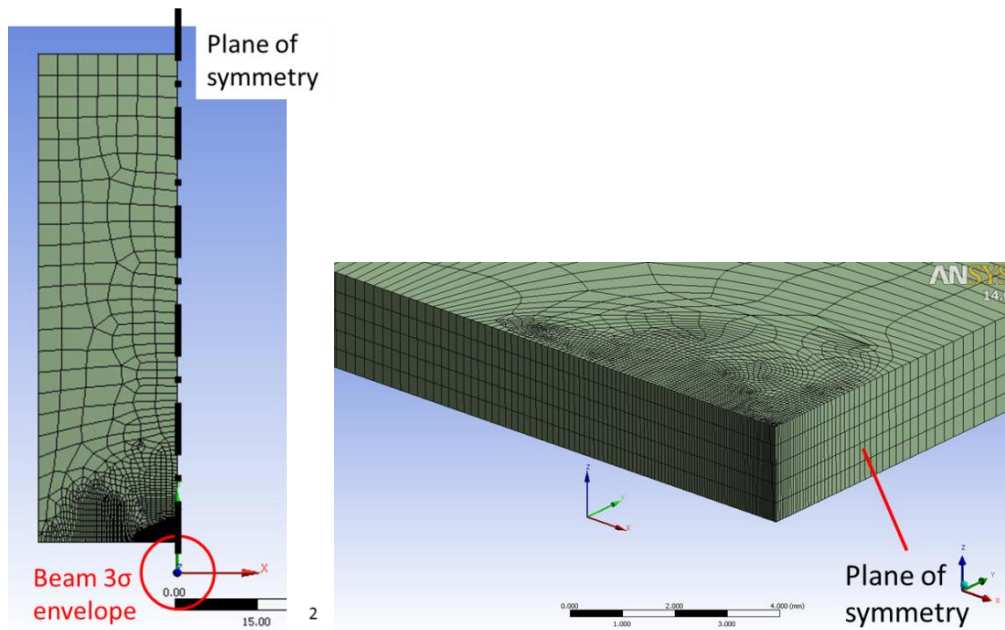


Figure 5: Finite element mesh

4.1.2 Beam Modeling

As the beam impacts the scraper, energy will be deposited over a longitudinal distance of order $20\mu\text{m}$ [3], or about 1% of the scraper thickness. For simplicity in modeling, we

conservatively assume that the energy is deposited directly on the surface (i.e. over a longitudinal distance of 0).

Based on the beam profile, a surface heat flux (in units W/mm^2) was calculated in Excel on a grid with $50\mu\text{m}$ pitch in both transverse directions (X and Y). Integrated over the area of the scraper, the scraped energy calculated by Excel was 62.56W. In Excel, a table with X,Y and surface heat flux was generated. This table was read into ANSYS and mapped onto the mesh using the built-in interpolation routine. The surface heat flux mapped onto the mesh and integrated over the area of the scraper had a total power of 62.94W, slightly higher than the Excel input. This interpolation error of $<1\%$ is negligible compared to other uncertainties in the analysis. The mapped surface heat flux is shown in Figure 6. The peak value is $18.4\text{W}/\text{mm}^2$.

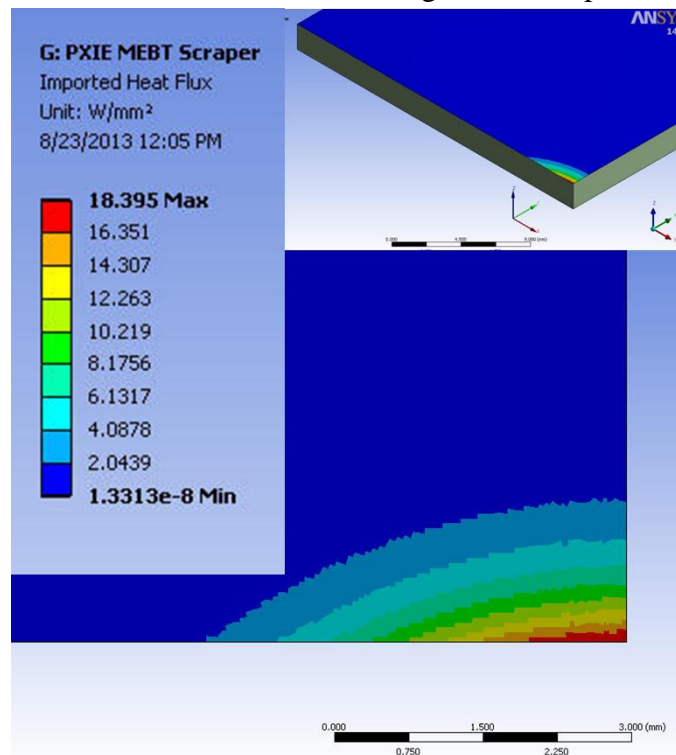


Figure 6: Beam-induced surface heat flux

4.1.3 Thermal Parameters

Heat rejection from the scraper was modeled as occurring only by radiation exchange with the environment. Only the two large $88.9 \times 50.6\text{mm}$ faces were assumed to radiate, radiation from the edges of the plate was neglected. Surface emissivity was set at 0.1 (constant with temperature), and the environment was assumed to be at a constant and uniform temperature of 300°K .

4.2 Temperature distribution and mechanical stresses

4.2.1 Steady State Thermal Analysis

A thermal analysis was performed to recover temperatures at steady state (thermal equilibrium). Results are shown in Figure 7. Peak temperatures approached 1200°C at the beam interaction region. The “cool” end of the scraper was still above 700°C, and would be contributing significantly to the radiative cooling.

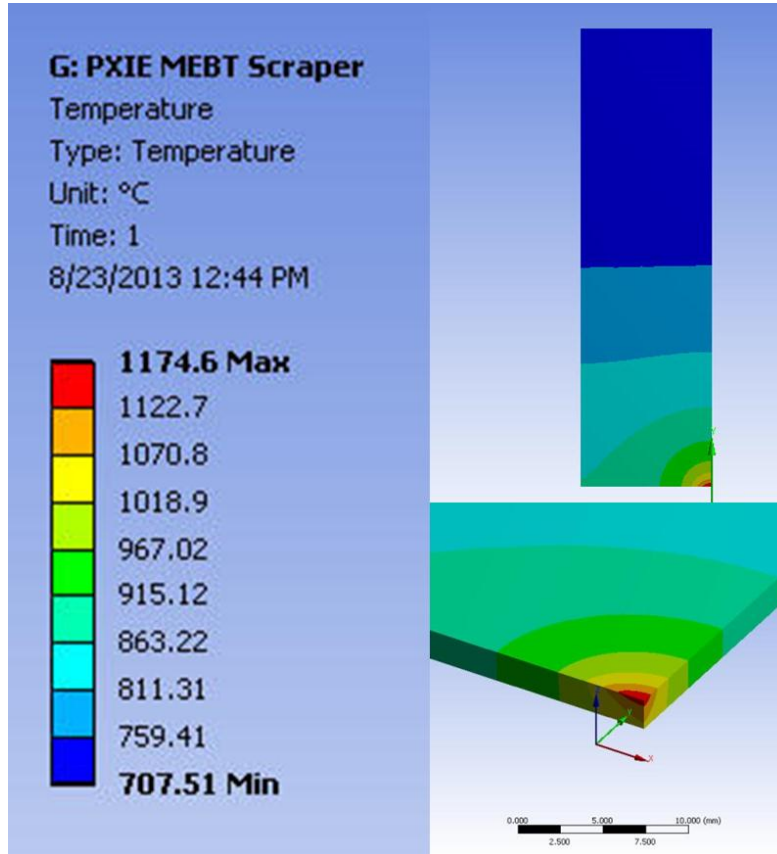


Figure 7: Steady State Temperature Profile

4.2.2 Structural Analysis

Steady-state thermal conditions were used as an input load to a stress model. No other loads (i.e. from supports, gravity, etc.) were considered. Stress and deflection conditions were recovered.

Von Mises' stress is a measure of “effective” stress from a complex tensor stress state, and is appropriate for ductile materials only. Though TZM is brittle at room temperature, it is more ductile at high temperatures. Peak Von Mises' stresses of 65MPa existed near the beam interaction region, as is shown in Figure 8. These stresses are dominated by compressive stress at the hot outer fiber of the scraper, where material heated by the beam attempts to expand thermally and is resisted by cooler surrounding material. Stress peaks at the surface of the material, where compression in the normal direction is (by definition) zero, and the resulting stress state is planar rather than hydrostatic.

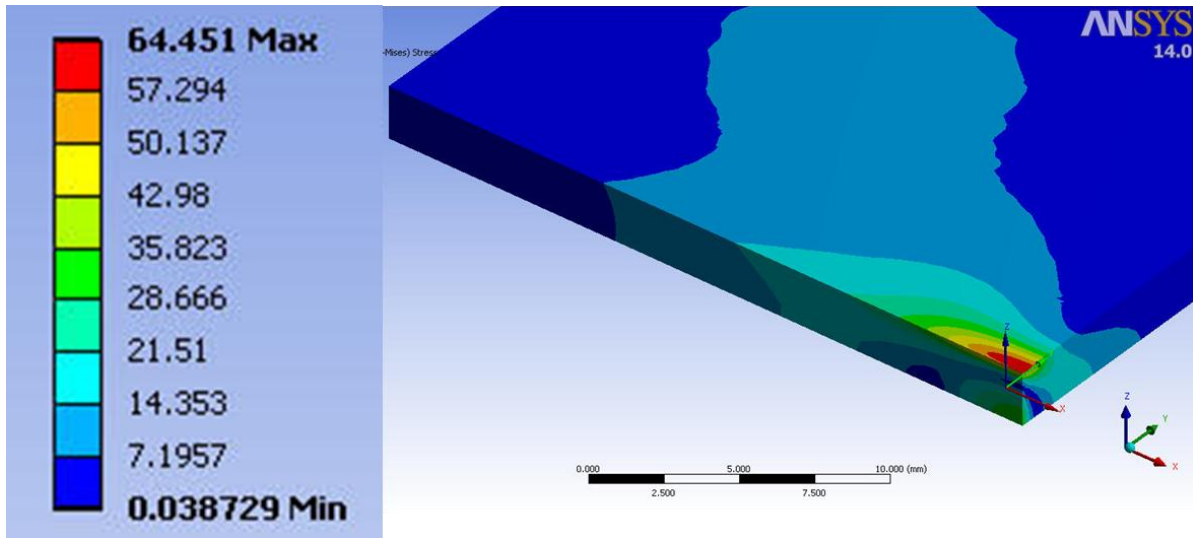


Figure 8: Von Mises' Stress near beam interaction region (MPa).

Maximum principal stress is a measure of the maximum tensile stress in any one direction at a given location in the material. It is significant for brittle materials that might tend to fail by crack propagation. Principal stress results are shown in the figure below and peak near the cooler back surface of the scraper. The compression driving the peak Von Mises' stress described above is reacted by developing a local area of tension on the back surface of the scraper. The maximum principal stress predicted is 35MPa.

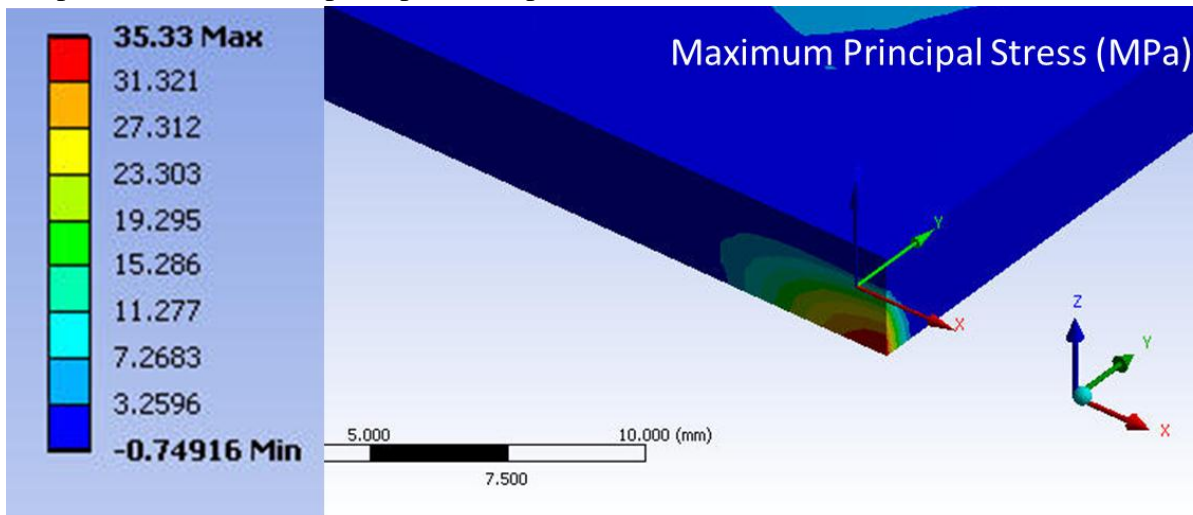


Figure 9: Maximum Principal Stress near beam interaction region (MPa)

The mechanical properties of TZM depend strongly on temperature, so one must consider not only the stress but the temperature at which it occurs. The Von Mises' stress and Principal Stress can be compared to a temperature-dependent yield curve, as shown in Figure 10. At the temperatures of interest, yield stress is above 400 MPa, though the temperature derivative is steep. Even so, the predicted temperature/stress conditions should be survivable.

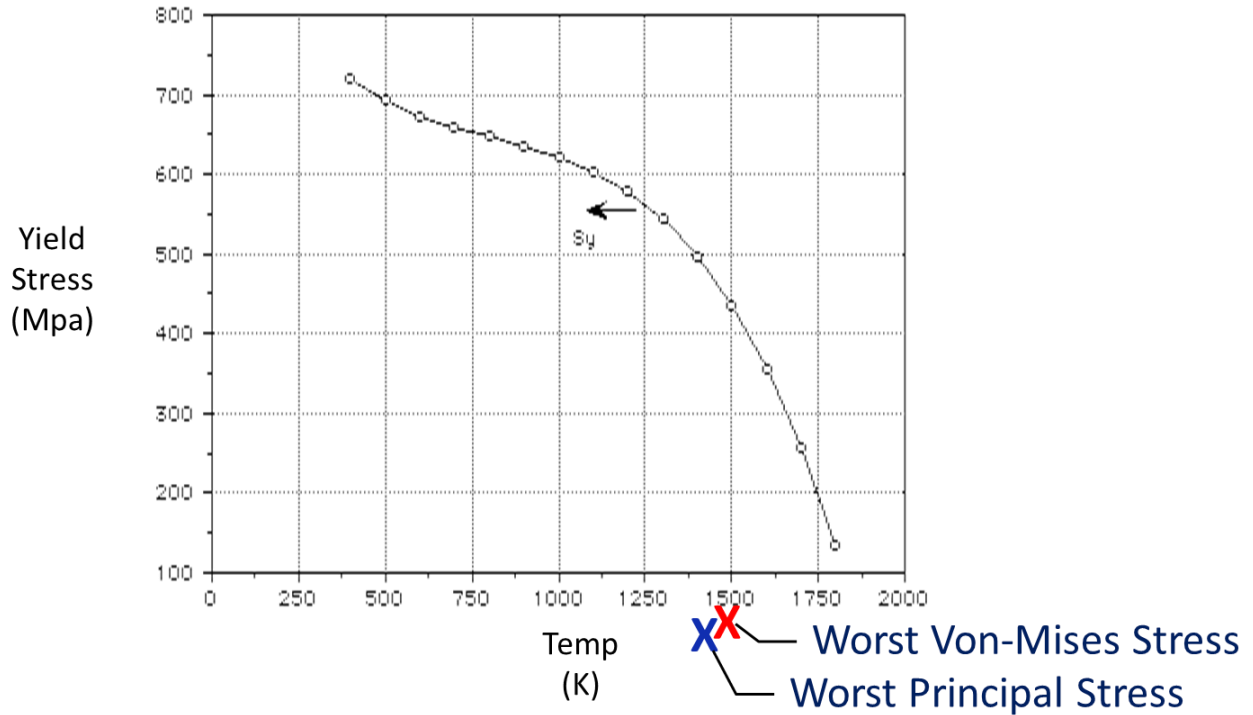


Figure 10: Stress/Temperature Conditions for TZM.

The structural model was also used to recover deflections of the scraper, which was supported from the “cool” end. The scraper expands transversely (into the beam) by 0.4mm.

4.3 Conclusions from the ANSYS simulations

The predicted steady-state temperatures of the scraper are high, but are within the capability range of TZM. As can be seen in Figure 10, the strength of TZM falls precipitously above ~1600°K, and if we were to simply extrapolate the curve, would go to zero at ~1900°K. So these temperatures should be avoided, but the predicted temperatures of ~1200°C/1500°K should be acceptable.

The predicted stress conditions of the scraper are acceptable. As a brittle material, the strength properties of TZM do depend on surface condition: cracks or flaws at the surface can propagate into the bulk and cause failure. The number, size and sharpness of these flaws should be minimized by the conventional techniques:

- Complete removal of any EDM recast layer
- Grinding the surface of the TZM with progressively smaller grit sizes
- Finish with fine Scotchbrite to create mid-scale roughness (to preserve higher emissivity)
- Electropolish to blunt flaws and reduce fine-scale roughness. In this particular application this practice may not be desirable due to the possibility of reducing emissivity

5 Testing of the scraper prototype with an electron beam

The scraper prototype was irradiated by an electron beam at a test stand developed for testing of the absorber prototype [7]. The tests had several goals:

- to estimate the emissivity of the TZM plate;
- to develop diagnostics tools for measuring the surface temperature by thermal radiation;
- to understand peculiarities of scraping a high-power density beam.

To fit the thermal radiation measurements, a C++ program simulating the scraper thermal regime was written. For simplicity, this program uses two-dimensional approximation, i.e., electrons are assumed to lose the energy evenly across the plate thickness. It was compared to ANSYS simulation at a large beam radius and showed a good agreement. The program allowed making fast estimations at various emissivity and power values.

5.1 Test stand

The test stand used in the experiments is shown in Figure 11, and its parameters are listed in Table 3. Using solenoids, the beam can be focused into a several-mm spot with nearly constant current density at the location of the scraper plate moved within several cm using dipole correctors. For calibration and cathode conditioning, the beam can be passed into a collector that captures 98% of the current. Alternatively, without breaking the vacuum either the absorber prototype or the scraper plate can be moved into the test chamber for irradiation by the beam.

Table 3. Electron beam test stand parameters

Beam parameters	
Current range	0.1-200 mA
Operational energy	27.5 keV
Vacuum without beam /with 190mA on absorber	
Gun (20 l/s ion pump)	$1 \cdot 10^{-10} / 1 \cdot 10^{-8}$ Torr
Test chamber (300 l/s turbo)	$1 \cdot 10^{-8} / 1 \cdot 10^{-7}$ Torr
Absorber prototype	
Material	Molybdenum TZM
Angle between the surface and the beam	~ 155 mrad
Water cooled	
Equipped with thermocouples	
Scraper prototype	
Material	TZM
Angle between the surface and the beam	$\sim 30^\circ$
Electrically isolated	
CCD camera	
Monochrome Progressive Scan CCD TM-9701, www.jai.com	
Resolution as assembled	0.24 mm/px
Optical transition Radiation (OTR) measurements	
Heat radiation measurements	

The surface of the object being tested can be observed through a 6" window (a quartz vacuum viewport with a led glass cover) by eyes or with a CCD camera. Camera images were captured and saved as images and text files with a dedicated program [8]. Code ImageJ [9] was extensively used for visual presentation of images and preliminary analysis.

The light from the surface has two major components: Optical Transition Radiation (OTR) and thermal radiation, which are discussed below.

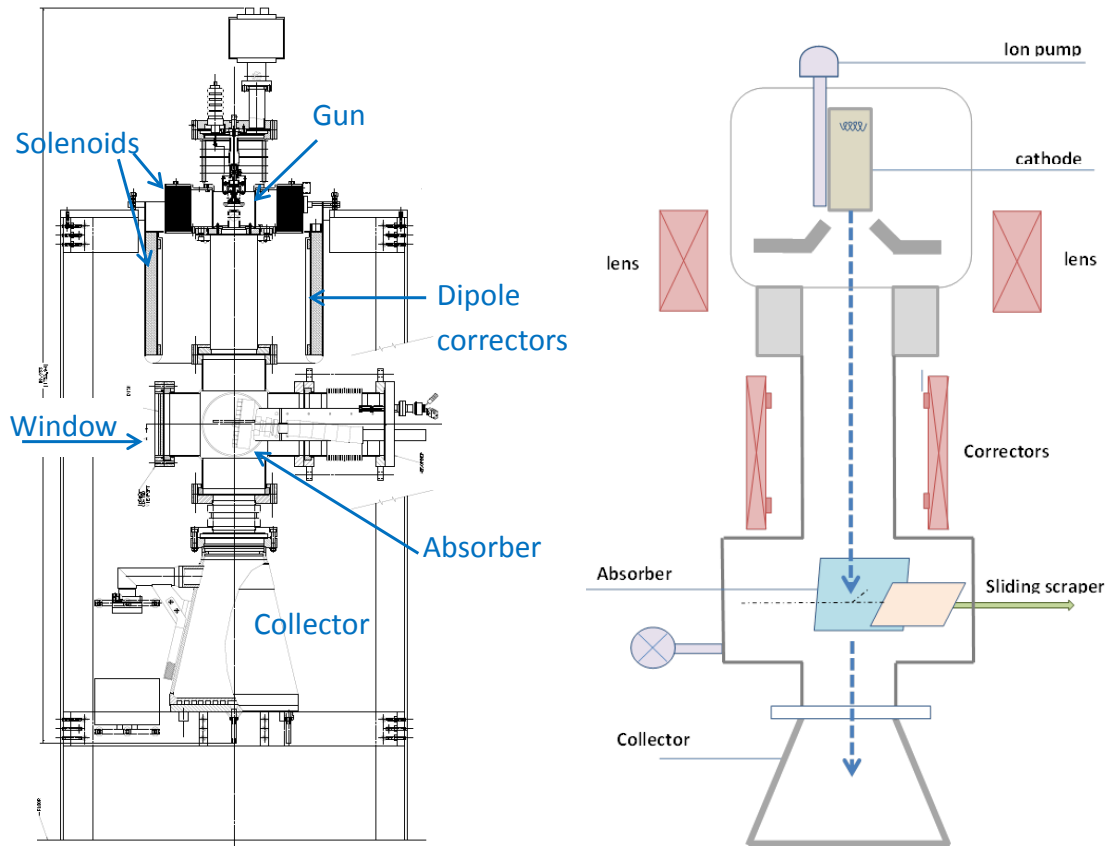


Figure 11: Drawing of the electron beam test stand and its simplified view from the window side.

5.2 OTR measurements

At low power density and short exposure times, the beam image was dominated by the OTR component. An indication of this mode is proportionality (after subtracting the background) of the light integral over the beam image to the beam current. An example of an OTR image is shown in Figure 12. For large beam sizes, an OTR image gives the footprint size and current density distribution.

An unexpected difficulty was a high intensity reflection of the light coming from the thermionic cathode. Without filtering, the image recorded by the camera was saturated, making unusable portion of the camera view field. In OTR measurements, the beam was typically moved as far from the reflection as dipole correctors allowed.

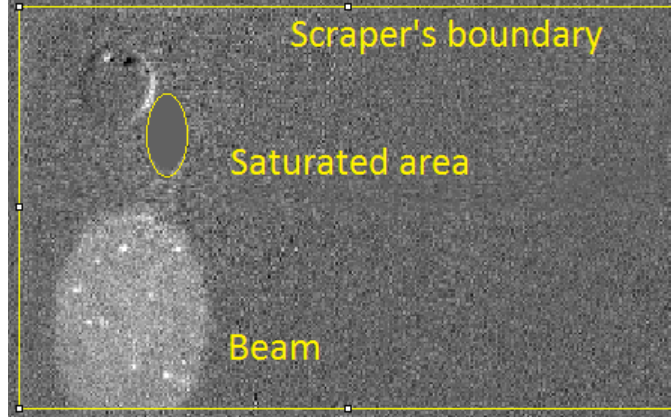


Figure 12. OTR measurements with subtracted background at 4.7 mA. Beam exposure time is about 1 second. The measured beam diameter is ~ 8 mm. The black spot is the result of image saturation caused by the cathode light. White spot is the beam OTR image. Ellipticity of the beam image corresponds to the angle between the beam axis and the plate surface of 32° .

5.3 Thermal radiation measurements

At surface temperatures above $\sim 600^\circ\text{C}$, contribution of the OTR becomes negligible in comparison with the thermal radiation. After this transition, generally speaking the surface temperature can be reconstructed from the thermal radiation using Planck's law. In its short wavelength limit, the Wien's distribution, the light intensity is

$$I(\nu, T) = \frac{2h\nu^3}{c^2} e^{-\frac{h\nu}{kT}}, \quad (2)$$

where h is the Planck constant, ν is the light frequency, c is speed of light, k is the Boltzmann constant, T is emitting surface temperature, I is the emitted intensity.

To exclude dependence of camera's sensitivity on wavelength, a narrowband red filter (707 nm, 10% bandwidth of 53nm) [10] was installed. In this case, the camera reading can be approximated as

$$I_C(T) = I_0 e^{-\frac{T_{eff}}{T}}, \quad (3)$$

where $T_{eff} = h\nu/k = 20350$ K. The coefficient I_0 in Eq. (3) is difficult to calculate directly, because it depends on camera sensitivity and geometrical parameters of the system. Initially, I_0 was deduced from previous measurements with the absorber prototype, which is equipped with multiple thermocouples. However, inconsistencies found later in the original version of the camera program created significant uncertainty in this value. In the analysis below, I_0 was used as a fitting parameter.

5.4 Power reflection

One of unknowns in these tests was the portion of the beam power taken away by secondary and reflected electrons (power reflection coefficient κ). The results of calculating this coefficient as a function of the incidence angle with a Monte-Carlo code CASINO [11] are shown in Figure 13. However, we have no information about how reliable is the code and use the results for

guidance only. In measurements with the absorber prototype, the measured power reflection coefficient was found to be significantly lower than predicted by Figure 13, $\kappa= 55\%$ at 80° . On the other hand, the coefficient of secondary emission measured from balance of currents from the TZM plate, 59% at 32° angle, is significantly higher than the code predicts. However, likely most of the latter discrepancy comes from slow secondary electrons, the generation of which critically depends on the state of the surface and is difficult to model. Hence, it is reasonable to expect the power reflection coefficient to be between $20\text{-}40\%$ (at 32°). In fitting to the experimental data, this coefficient was used as a fitting parameter.

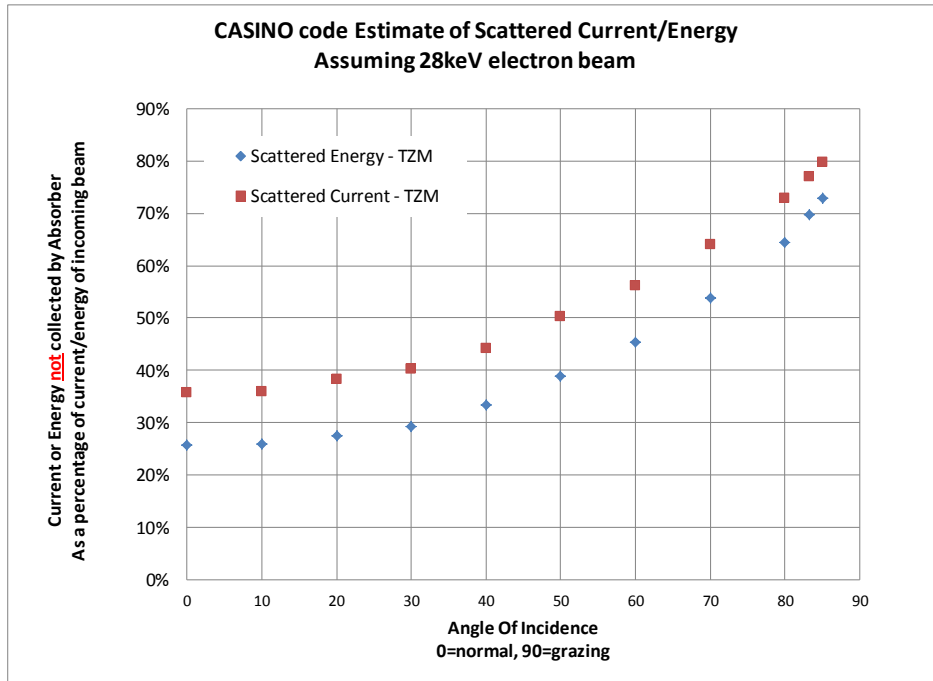


Figure 13. Portions of current and power of an electron beam reflected from a TZM surface as a function of the incident angle. Simulation by CASINO code [11].

5.5 Measurements with a large size beam

The first set of measurements was made with a large-size, low-current beam, where the OTR image gave information about the beam size. The current density distribution was found to be nearly constant (within the noise level), and simulations used the uniform model.

A complete analysis was applied to two runs, at $\sim 5\text{mA}$ and $\sim 4\text{mA}$ of the beam current. First, the OTR image was saved at each current, and then the red filter was installed. In each run, the plate was brought to thermal equilibrium, and the steady state image was recorded. The program allowed to report at $\sim 1\text{Hz}$ the integral of intensity over a rectangle. For these runs, the $\sim 6\text{mm} \times 6\text{mm}$ rectangle was selected in the center of the beam (Figure 14). The beam was turned off by a jump, and the cooling curve was recorded as shown in Figure 15.

For each of these runs, two curves were compared with simulations: a spatial intensity distribution in a steady state and temporal dependence of light intensity during cooling after turning beam off.

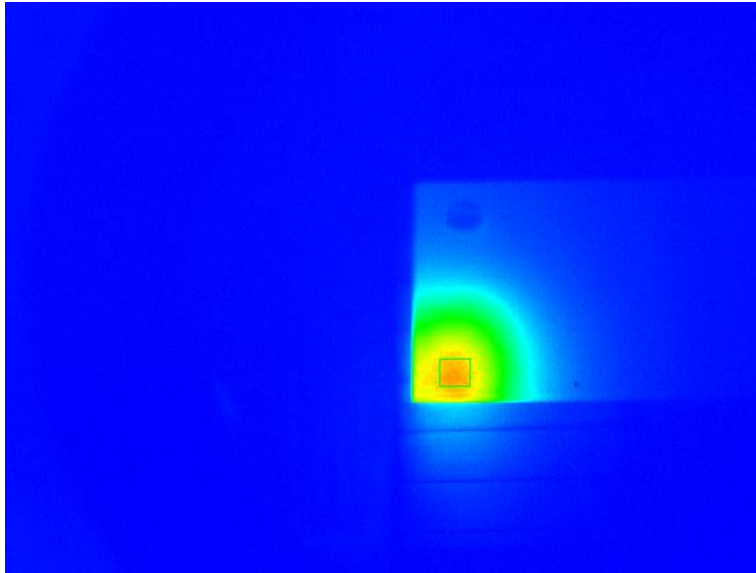


Figure 14. Screenshot of the camera program window in a steady state with ~ 5 mA beam. The light intensity is presented by false colors. The rectangle (26 x 23 pixels) designates the area from which the intensity integral was reported. The image outside of the plate is the light from the opposite side of the plate is reflected from the absorber prototype surface. Red filter installed.

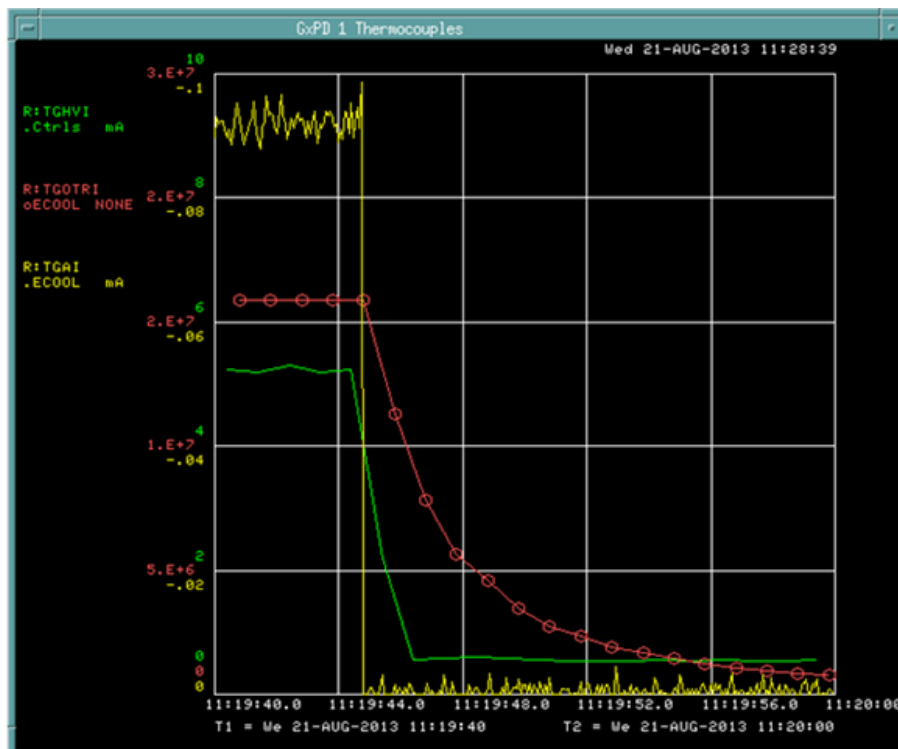


Figure 15. Cooling from the equilibrium state after heating the plate with 4.7 mA beam as shown in Figure 12. Green – cathode current (2 mA/div, 0.6 mA offset, 1Hz). Yellow – plate current (as measured, i.e. without taking into account secondary emission; 0.4 mA/div, 15 Hz). Red – light intensity from a rectangle shown in Figure 14 (1 Hz). The horizontal axis represents time, 4s/div.

5.5.1 Steady state spatial distribution

Spatial light intensity distribution was taken from images recorded in a steady state. Specifically, the data along a line coming through the highest temperature point (the yellow line in Figure 16) were compared with simulations.

A set of computer simulations with the C++ code was run at the same beam parameters and various combinations (ϵ , κ) of the emissivity and power reflection coefficient. The resulting temperature distribution along the same line was used for fitting the measured intensity distribution by Eq. (3) with I_0 as a fitting parameter. An example of fitting is shown in Figure 17.

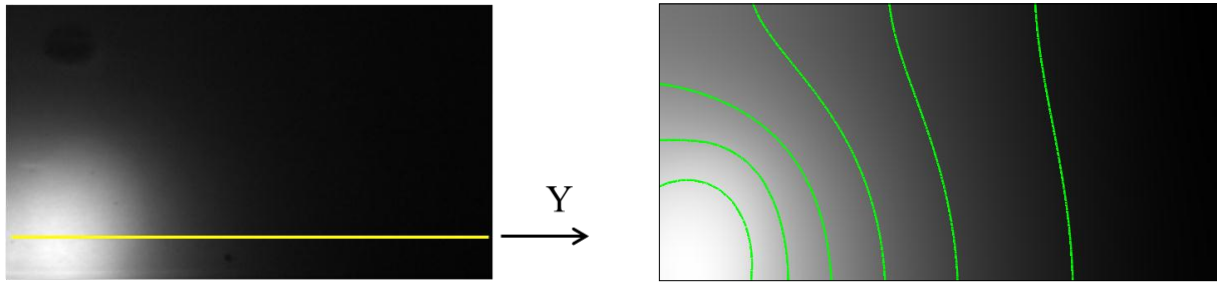


Figure 16. Left: image of the plate in a steady state (10 minutes of beam exposure time). Beam parameters as for Figure 12. The image was recorded with the narrowband red filter (707 nm). Right: simulation for the same parameters with the C++ code. The green lines represent contours of constant temperature (100K between neighboring lines).

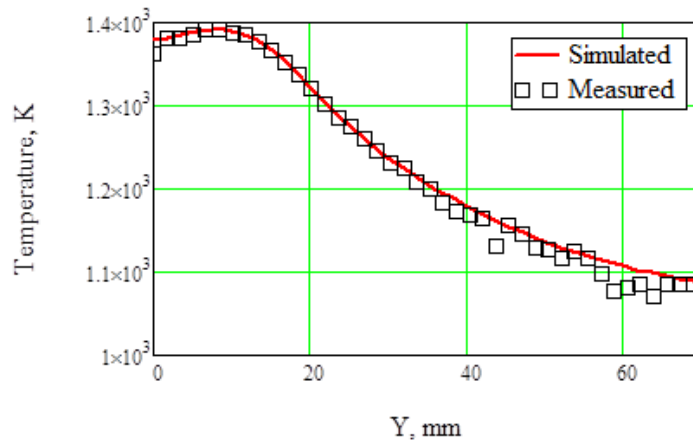


Figure 17. Comparison of measured and simulated temperature distributions along the line shown in Figure 16. Emissivity is 0.11, power reflection coefficient is 0.1.

5.5.2 Temporal temperature dependence

As seen from Figure 17, the temperature distribution has a plateau near its maximum in steady state, and during cooling this distribution is even smoother. Therefore, the integral of the light intensity over a small rectangle in this region gives a reasonable representation of the maximum temperature. Similarly to the spatial case, the measured data were fitted to simulations using (ϵ ,

κ, I_0) sets as fitting (Figure 18). Note that though the beam is off during recording these data, the power reflection coefficient still affects the fitting through parameters of the initial (steady state) temperature distribution.

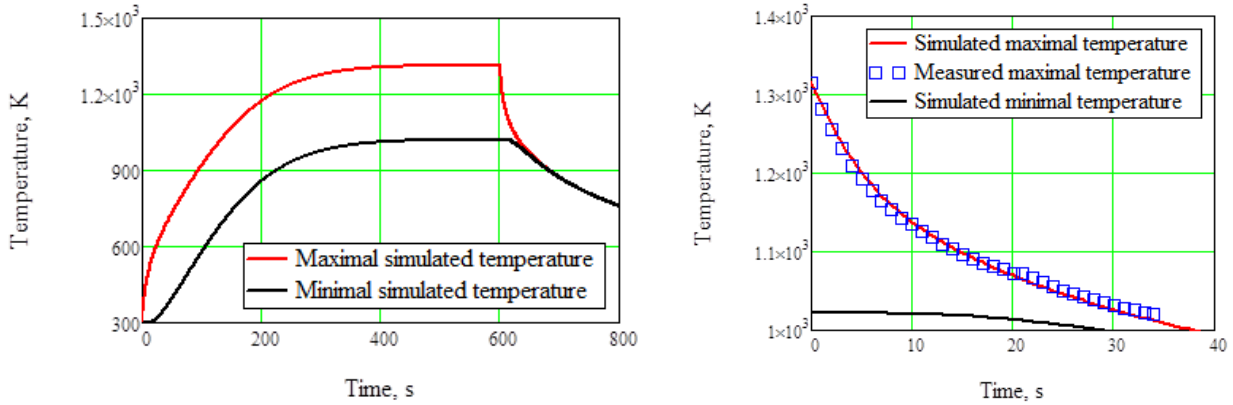


Figure 18. Comparison of measured and simulated temperature temporal behavior during plate cooling. Left: simulation of maximum and minimum temperatures of the plate after turning the 5mA beam on at $t=0$ and turning it off after 10 minutes. $\epsilon = 0.12, \kappa = 0.2$. Right: fitting the intensity integral to the simulated decrease of the maximum temperature for the same parameters.

5.5.3 Results of measurements with the large beam

Four analyzed light intensity curves can be simultaneously fit well (within statistical fluctuations) to simulations with multiple combinations of (ϵ, κ) , each of them corresponding to a specific value of I_0 . In Table 4 these sets are presented with the maximum temperature on the plate shown instead of I_0 . Figure 19 shows the same data graphically.

Table 4. Sets of parameters giving the best fit to experimental data.

k (power reflection)	0.0	0.1	0.2	0.3
ϵ (emissivity)	0.11	0.12	0.13	0.14
T_{\max}, K	1446	1368	1292	1215

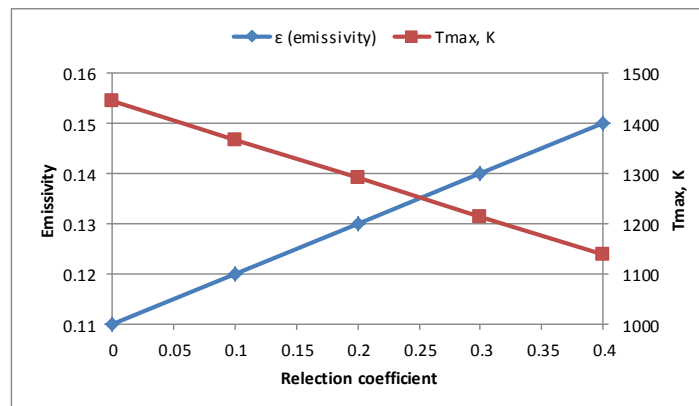


Figure 19. Relationship between the reflection coefficient, emissivity, and optical system calibration (shown as the maximum temperature on the plate). Data for $\kappa=0.4$ are from linear fits.

While the procedure by itself gave a range of parameters rather than a unique best-fitting set, the ambiguity in the value most important for future design of scrapers, emissivity, is acceptable. Moreover, if one follows reasoning in Section 5.4 and limits the range of the possible power reflection coefficient to 0.2 -0.3, emissivity is determined to be 0.13 – 0.14, similar to what is typically cited in literature (e.g. [4]).

5.6 Scraping of a high-power-density beam

To model scraping of a high-power-density beam, electrons were focused into ~2 mm radius spot in the location of the scraper edge. The beam size at the current of ~80mA was assumed the same as it has been found in previous measurements with the absorber prototype with the same focusing parameters in the same location. The scraper was moved into the beam so that the collector current dropped by several mA. The increase of the scraped current as a function of the scraper shift was consistent with ~2 mm beam radius.

The most detail measurements as well as ANSYS simulations were performed for the case of 5mA.

5.6.1 ANSYS simulation for the test stand case of high-power-density beam scraping

In this ANSYS simulation, the scraper model was similar to what has been described in Section 4.1.1 but the beam was assumed to be with a constant current density. The 80 mA beam radius was 2.2 mm, so that the scraper edge moved into the beam by 0.5 mm intercepted 5 mA. The beam was coming to the plate at 30° to the surface. Emissivity and the power reflection coefficient were assumed as found in measurements, 0.13 and 0.2, correspondingly. 80% of the intercepted power, or 109W, was absorbed. The simulated steady state distribution is shown in Figure 20. Note that the maximum power density was 57 W/mm².

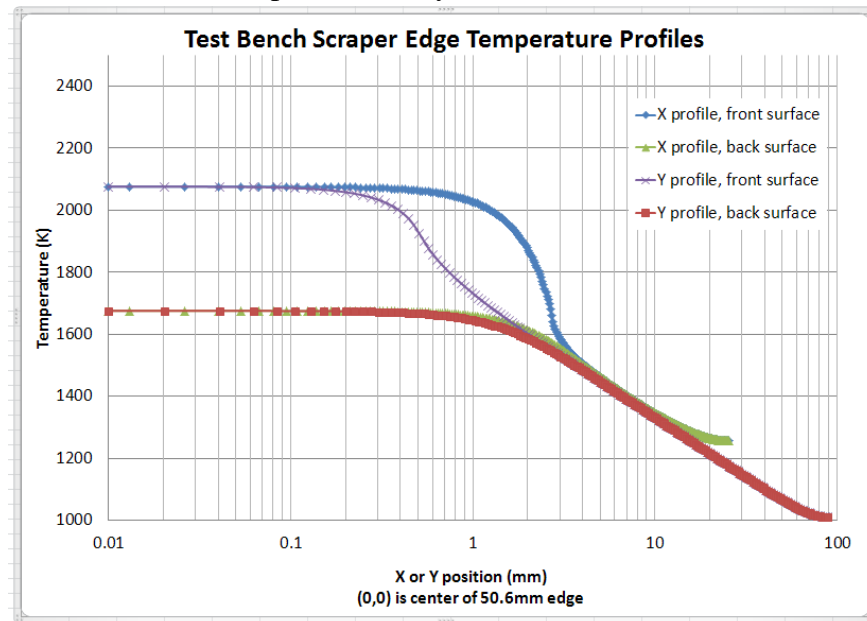


Figure 20. Steady state temperature distribution simulated by ANSYS for the case of scraping a high-power-density beam at the test stand. X is along the 50.6 mm edge, and Y lies at the symmetry line of the plate.

5.6.2 Measurements of high-power-density beam scraping

An example of parameter variation during a typical measurement with high-power-density beam scraping is shown in Figure 21. First, the electron beam is turned on, and a program [12] is set to maintain its current at 80 mA by adjusting the potential of the gun control electrode (indicated by arrow 1 in Figure 21). The collector current is 98% of the gun current, in accordance with geometrical efficiency. Then the scraper is moved into the beam (arrow 2), the collector current drops by ~ 5 mA, while the plate current increases by ~ 2.5 mA (in agreement with the secondary emission coefficient of ~ 0.5). Heating of the plate results in its thermal expansion, and the scraper edge moves into the beam even further. Arrow 3 indicates a moment when an operator moves the beam slightly away from the scraper with dipole correctors to keep the scraped current at ~ 4.5 mA (in this specific case). At a later moment (arrow 4), the light measuring rectangle in the program was adjusted to cover the entire plate. With the plate being heated up, the light integral increases, dropping in the moments of shifting the beam away (arrow 5). In ~ 15 min after beginning of scraping, the system comes into a steady state.

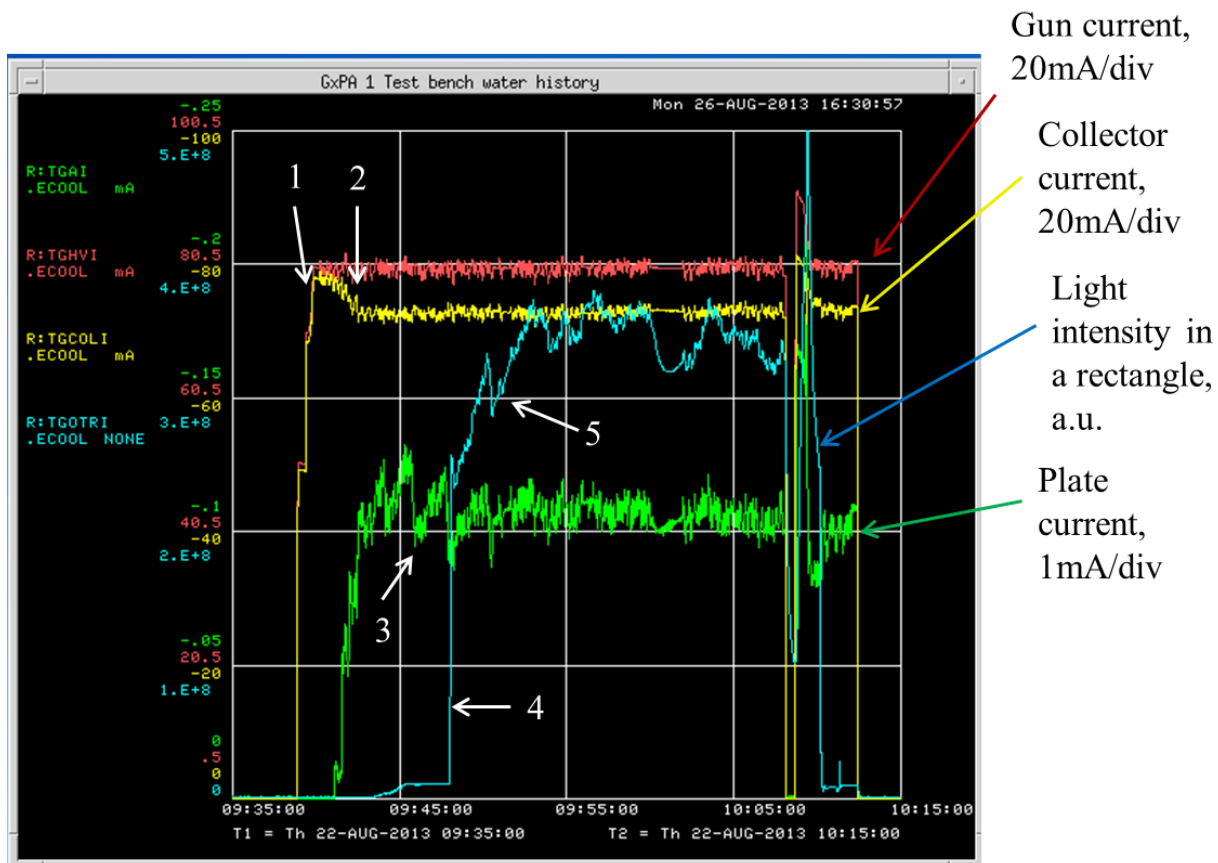


Figure 21. Parameters variation during a typical measurement with high-power-density beam scraping. Horizontal axis – time, 10 min/div. Red filter.

A set of successive images recorded while the plate was heating up is shown in Figure 22. From the very first image, the image is saturated in the central area of the beam footprint. To extend the available intensity range, the measurement was repeated at the same beam parameters

(with the scraped current of $\sim 5\text{mA}$) with the red filter only; the red filter and neutral filter with 10% transmission; and with the red filter and neutral filter with 1% transmission. The distributions along the central line from steady state images was combined with corresponding coefficients ($\times 1$, $\times 10$, and $\times 100$) and compared with the simulations (as in Figure 20, curve “Y profile, front surface”) using calibration for the coefficient I_0 found in measurements in Section 5.5.3 for $\varepsilon = 0.13$, $\kappa = 0.2$.

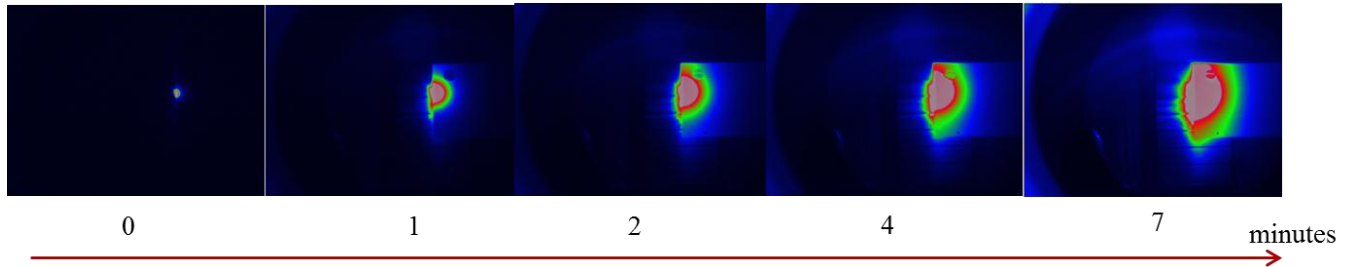


Figure 22. Successive camera images in false colors during heating the plate. The image on the left of the scraper edge is interpreted as reflection of the light emitted by the back side of the plate from the surface of the absorber prototype. The first image is recorded immediately after inserting the scraper into the beam (roughly corresponds to the moment indicated by arrow 2).

The result of the comparison is shown in Figure 23. The only additional fitting the position of the scraper edge. In all images, including without filters and with a bright external light, the edge looked smeared out by several pixels. Taking into account a sharp rise of the temperature toward the edge found in simulations and comparatively large distance at the plate corresponding to a single pixel (0.24mm), smoothing of the peak temperature by this imperfection of focusing seems natural. Numerically, the best fit, shown in Figure 23, corresponds to 1 mm distance between the point with the highest light intensity in the recorded image and the simulated plate edge.

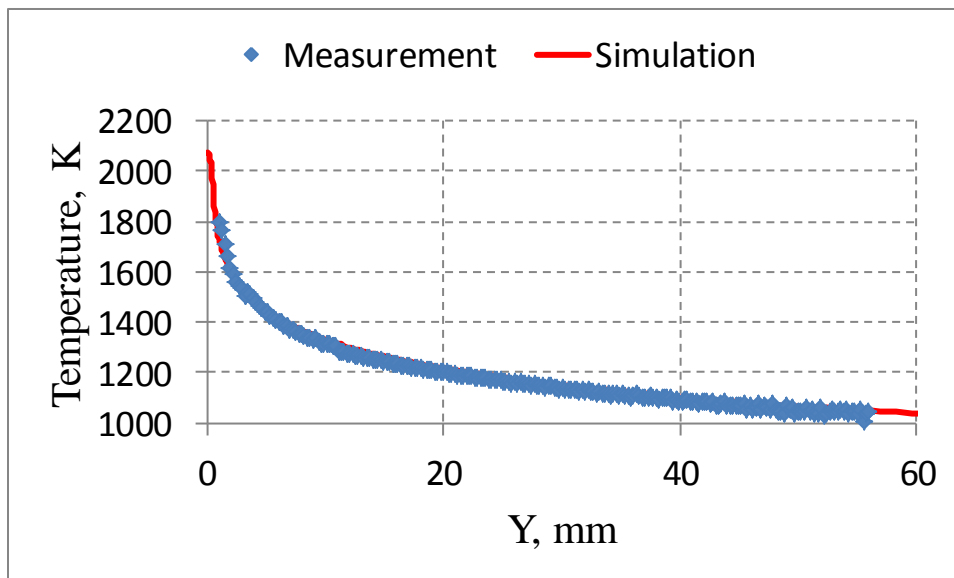


Figure 23. Comparison of the temperature distribution restored from three images recorded with different filters and the simulated curve.

The maximum current scraped in this mode was $\sim 5\text{mA}$ in a steady state and $\sim 6\text{mA}$ for several minutes. Visual inspection through the vacuum window did not reveal any modifications (e.g. melting, discoloration) of the plate surface.

6 Discussion

A radiation-cooled scraper seems to be a good option for at least initial commissioning of PXIE. In the simplest version, the scraper would be an electrically isolated TZM plate with a linear drive. An attractive possibility is to re-use the linear drives that have been used in the Electron cooler.

Another positive feature of this option is that as a result of combination of high diffusion of protons in TZM and high operating temperature, blistering will be highly unlikely.

Finally, the design is tolerant to errors because of a high melting point of TZM and simplicity of the design. Figure 10 suggest the maximum working temperature $\sim 1600\text{ K}$, and this should be used as a basis for the scraper design. However, no visible damage was found even though the plate was subjected to significantly higher temperatures of $\sim 2000\text{K}$ as in Figure 23. Probably, it takes more time than tens of minutes in these measurements for the loss of mechanical strength in a small area to result in a significant deformation. In practice, it means that the protection system and facility operators can have enough time to react if the power rating of a scraper (likely $\sim 50\text{ W}$) is accidentally exceeded. Moreover, with no water cooling, a deformation or even partial melting of the plate would not result in a dramatic damage to the rest of the facility.

Obviously, the radiation-cooled option has several negative features as well. The most significant may be the uncertainty of the scraper edge position caused by thermal expansion. Simulations of Section 4 predict a shift of 0.4 mm , and in tests with scraping of a high-power-density electron beam similar displacements were observed experimentally. The solution can be similar to what was used (manually) at the test stand: an automated feedback system that operates the linear drive to preserve the current to the scraper within specified limits.

Another undesirable feature is a possible cross-talk between 4 scrapers in the same enclosure because part of radiation would be intercepted by neighboring plates. Specific value of de-rating of the scraper operational power depends on design specifics.

Finally, radiation brings the heat to the vacuum walls, which may result in the necessity to water-cool them.

7 Summary

1. Simulations and tests with an electron beam show that a radiation-cooled scraper is feasible for PXIE MEBT parameters. If a TZM plate with similar dimensions is used as a scraper, its power rating can be $\sim 50\text{ W}$ per jaw.
2. Emissivity of the TZM plate was found to be ~ 0.13 .
3. Tools and procedures for measuring the plate temperature by analyzing thermal radiation were developed.

8 Acknowledgements

Authors acknowledge an important contribution of R. Thurman-Keup who modified the camera-reading program to needs of the tests and participation of L. Prost and B. Hanna in some of the measurements.

9 Bibliography

- [1] "Project X Reference Design Report," 2013. [Online]. Available: <http://projectx-docdb.fnal.gov/cgi-bin/ShowDocument?docid=776>.
- [2] "PXIE Design Handbook," 2013. [Online]. Available: <http://projectx-docdb.fnal.gov/cgi-bin/ShowDocument?docid=1148>.
- [3] C. Baffes et al, "Design Considerations for an MEBT Chopper Absorber of 2.1MeV H- at the Project X Injector Experiment at Fermilab," in *Proc. of IPAC'12*, New Orleans, USA,2012, WEPPD035.
- [4] "Table of emissivity of various surfaces," [Online]. Available: http://www-eng.lbl.gov/~dw/projects/DW4229_LHC_detector_analysis/calculations/emissivity2.pdf.
- [5] [Online]. Available: www.ansys.com.
- [6] "ITER materials property literature survey for TZM," [Online]. Available: <http://www-ferp.ucsd.edu/LIB/PROPS/PANOS/moa.html>.
- [7] C. Baffes and A. Shemyakin, "Status of PXIE MEBT absorber development," 2013. [Online]. Available: <http://beamdocs.fnal.gov/AD-public/DocDB/ShowDocument?docid=4362>.
- [8] The program was written and modified for this test's needs by R. Thurman-Keup.
- [9] "ImageJ," [Online]. Available: <http://rsbweb.nih.gov/ij/>.
- [10] Melles Grios, <http://www.cvimellesgriot.com/> . All filters were provided to us by V. Scarpine and A. Lampkin.
- [11] "CASINO, a MC code from Université de Sherbrooke, Québec, Canada," [Online]. Available: <http://www.gel.usherbrooke.ca/casino/index.html>.
- [12] The Finite State Machine program was written and maintained by L. Carmichael. .